ISSN 1023-1935, Russian Journal of Electrochemistry, 2017, Vol. 53, No. 1, pp. 25–38. © Pleiades Publishing, Ltd., 2017.
Original Russian Text © G.R. Nasretdinova, R.R. Fazleeva, Yu.N. Osin, A.T. Gubaidullin, V.V. Yanilkin, 2017, published in Elektrokhimiya, 2017, Vol. 53, No. 1, pp. 31–45.

Methylviologen-Mediated Electrochemical Synthesis of Silver Nanoparticles via the Reduction of AgCl Nanospheres Stabilized by Cetyltrimethylammonium Chloride

G. R. Nasretdinova[a], R. R. Fazleeva[a], Yu. N. Osin[b], A. T. Gubaidullin[a], and V. V. Yanilkin[a, *]

[a] *Arbuzov Institute of Organic and Physical Chemistry, Kazan Research Center, Russian Academy of Sciences, Kazan, 420088 Russia*

[b] *Kazan (Volga region) Federal University, International Center "Analytical Microscopy", Kazan, 420018 Russia*

**e-mail: yanilkin@iopc.ru*

Received January 12, 2016

Abstract—Efficient synthesis of silver nanoparticles stabilized by cetyltrimethylammonium cations ($Ag@CTA^+$) is carried out in aqueous medium by methylviologen-mediated electroreduction of silver chloride nanospheres stabilized by surface-active CTA^+ cations ($AgCl@CTA^+$, diameter ~330 nm), on a glassy carbon electrode at potentials of the $MV^{2+}/MV^{\bullet+}$ redox couple. The nanospheres $AgCl@CTA^+$ can be reduced immediately on the electrode at a low rate and the resulting metal is deposited on the electrode. In the mediated reduction, the metal is not deposited on the cathode but the quantitative reduction of AgCl to $Ag@CTA^+$ nanoparticles proceeds completely in solution volume at the theoretical charge. In aqueous solution, the nanoparticles are positively charged (electrokinetic (zeta) potential is +74.6 mV), their characteristic absorption maximum is at 423 nm and the average hydrodynamic diameter is 77 nm. Isolated Ag@CTACl nanoparticles have the size of 39 ± 15 nm. The preferential form of metal nanoparticles is sphere with the diameter of 34 ± 24 nm; nanorods are also obtained in small amounts (4%); the average size of metal grains is 8–16 nm.

Keywords: electrosynthesis, nanoparticles, nanosphere, nanorod, silver, reduction, silver chloride, mediator, methylviologen, stabilizer, cetyltrimethylammonium chloride

DOI: 10.1134/S1023193517010098

INTRODUCTION

Recently, small and ultrasmall metal particles progressively attracted attention due to their unusual properties and the wide diversity of their potential applications in catalysis, electronics, biomedicine, optics, analysis, etc. [1–7]. Their best developed and most widely accepted synthesis is the chemical reduction of metal ions and complexes in solution by various reducers. Electrochemistry is used rarely for synthesizing metal dispersions (sols). This is explained primarily by the fact that as a rule the metals generated by reduction of their ions and complexes are deposited on the electrode surface. In the presence of stabilizers of metal nanoparticles (NP), the fraction of deposited metal decreases but still remains sufficiently high. Thus, when silver NP are synthesized by the reduction of silver ions in the presence of polyvinylpyrrolidone widely used for stabilization of metal NP, the fraction of deposited metal reaches 80% [8, 9]. Hence, all the methods developed for electrosynthesizing metal NP in the solution volume should solve in one way or another the problem of their deposition. Thus, the method of pulsed sonoelectrochemistry [10–12] combines the accumulation of NP on the electrode surface during short-term electroreduction with their subsequent transition to solution by supersonic treatment of the electrode. Reetz et al. [13–22] carried out the electroreduction of ions in aprotic organic media by using surface-active tetraalkylammonium or phosphonium cations as the supporting electrolyte. For the same purpose, we have proposed to use the mediated synthesis [23–32] the difference of which from aforementioned electrochemical methods is that the stage of metal ion reduction is transferred from the electrode surface to the solution bulk. In the process, the mediator is reduced on the cathode and its reduced form diffuses to solution bulk where reduces a metal ion or complex. This either completely eliminates or minimizes the metal deposition on the electrode. The efficiency of this method was recently demonstrated for the synthesis of NP of Pd [23–27], Ag [28, 29], Au [32], Co [31]. By means of this method, metal NP were synthesized in the absence and in the presence of stabilizers in aqueous, water-organic, and nonaqueous media from metal salts and complexes or by in situ generation of metal ions in solution at the metal anode dissolution during electrolysis.

Insofar as the stage of metal ion reduction does not proceed on the electrode, in contrast to other electrochemical methods, the method of mediated elec-

trosynthesis represents also a fundamentally new possibility of generating and synthesizing metal NP in processes where the metal ion reduction on the electrode is either hindered or impossible, e.g., as a result of insolubility or limited solubility of their salts, at their incapsulation in micelles, polymer globules or other matrices, immobilization on nonconducting solid supports, or when the cathode and the salt are in different liquid phases. One of these possibilities was demonstrated for electrosynthesis of nanocomposite materials silicate-core/silver-shell by methylviologen-mediated reduction of insoluble salt AgCl [30]. The present study provides experimental substantiation to yet another possibility of mediated synthesis of metal NP involving encapsulation of their salts in micelles by the example of preparation of silver NP in aqueous medium via the methylviologen-mediated reduction of AgCl nanospheres stabilized by the shells formed by surface-active cetyltrimethylammonium cations ($AgCl@CTA^+$).

EXPERIMENTAL

In this study, we used the methods of cyclic voltammetry (CV),dynamic light scattering (DLS), preparative electrolysis, scanning electron microscopy (SEM), scanning transmission electron microscopy (STEM), powder X-ray diffraction, and UV-visible spectroscopy.

Reagents and Working Solutions

Methylviologen dichloride $MV^{2+}\cdot 2Cl^-$ (Acros Organics), $AgNO_3$, cetyltrimethylammonium chloride (**CTACl**, Acros Oraganics), and NaCl were used without additional cleaning. Twice distilled water was used as the solvent.

The solution of $AgCl@CTA^+$ nanospheres used in CV, DLS, and preparative electrolysis was prepared by the well-known procedure [33] by adding drop-wisely 300, 150 and 1200 μL of aqueous solution of $AgNO_3$ (0.05 M) to 5, 2.5, and 20 mL of aqueous solution of cetyltrimethylammonium chloride CTACl (0.02 M), respectively, on active stirring by a magnetic stirrer. The solution remained transparent for a long time and became opaque in the end of drop-wise addition but remained homogeneous. The final concentration was as follows: 2.8 mM (0.40 g/L) AgCl, 18.7 mM CTA^+, 15.9 mM chloride ions, and 2.8 mM nitrate ions. During the further stirring for 1 h 20 min, the solution became white.

Solution of AgCl (2.8 mM (0.40 g/L)) was synthesized by a similar procedure by adding in drops the aqueous $AgNO_3$ (0.05 M) solution to the aqueous solution of sodium chloride (0.02 M).

Solution used in all electrochemical experiments were neutral (pH 6–7), no supporting electrolyte was added, and conductivity was provided by solution components.

Cyclic voltammograms (CV curves) were recorded by means of a potentiostat P-30S (Elins, Russia) (without *IR* compensation) in nitrogen atmosphere at the potential scan rate from 10 to 200 mV/s. A glassy carbon (**GC**) disk electrode (diameter 3.4 mm) pressed into perfluorinated polymer was used as the working electrode. The electrode was cleaned by mechanical grinding before each measurement. A Pt wire served as the counter electrode. The potentials were measured and are shown with respect to the aqueous saturated calomel electrode (SCE) connected with the working solution by a bridge filled with supporting electrolyte and having the potential of –0.41 V with respect to E_0' (Fc^+/Fc). The temperature was 295 K.

Preparative electrolysis was carried out in a diaphragm (porous glass) three-electrode glass cell under potentiostatic conditions in argon atmosphere at room temperature ($T = 295$ K) by means of P-30S potentiostat. During electrolysis, the solution was stirred by a magnetic stirrer. The working electrode represented a glassy-carbon plate ($S = 3.5$ cm^2); the SCE reference electrode was connected with the working solution by a bridge with supporting electrolyte. The counter electrode represented a Pt wire immersed in supporting electrolyte solution. After the end of electrolysis, the solution was studied by the CV method on an indicator GC electrode (diameter 3.4 mm) immediately in the electrolysis cell and also by UV-visible spectroscopy.

The samples for studying the $Ag^0@CTACl$ particles formed in electrolysis by the methods SEM, STEM, and powder X-ray diffraction, and also for measuring the electrokinetc (zeta) potential of particles were prepared as follows. The solution after electrolysis was centrifuged for 2 h at the rate of 15000 rpm; in the process, every 0.5 h, the maximum possible volume of liquid was removed from the precipitate surface. The solution over the precipitate was of lemon color. In the final system, a small layer of liquid remained on the precipitate. This suspension was studied by the powder X-ray diffraction method. For SEM, STEM, and zeta-potential determination, the suspension was dispersed in distilled water by sonication. For SEM, the resulting solution was placed on the surface of titanium foil preliminarily cleaned by sonication in water and acetone. Then, the sample was dried in air on gentle heating (to 40°C). For STEM, the solution was placed on the surface of 3-mm copper grid covered by a formvar film and then dried.

For studying nonstabilized Ag^0 particles, the solution after electrolysis was centrifuged for 0.5 h at a rate of 15000 rpm; solution over the precipitate was transparent. The precipitate was washed with water and then dispersed in distilled water. The resulting solution was prepared to its analysis by SEM and STEM methods by the procedures described above.

DLS method was used for measuring the hydrodynamic diameter and the zeta potential of particles in solutions. The measurements were carried out with the use of Malvern Instrument Zetasizer Nano setup (Mal-

vern Instruments, UK). The measured autocorrelation functions were analyzed by programs Malvern DTS.

Electron-microscopic analysis. The morphology of samples was studied on high-resolution scanning electron microscope Merlin (Carl Zeiss, Germany) equipped with ASB, SE, and STEM detectors. The elemental analysis was carried out by means of EMF detector AZTEC X-MAX (Oxford Instruments, UK) combined with a microscope.

X-ray diffraction measurements of samples were carried out on automatic X-ray diffractometer Bruker D8 Advance (Germany) with the attachment Vario and the linear coordinate detector Vantec. We used Cu$K_{\alpha 1}$ radiation ($\lambda = 0.154063$ nm) monochromatized by a Johansson curved monochromator; the X-ray tube working mode was 40 kV, 40 mA. Powder diffraction patterns were obtained at room temperature in the Bragg-Bretano geometry with a flat sample.

The sample in its liquid form was placed on a silicon plate which reduced the background scattering. Once the layer was dried, several layers were applied on it to increase the total amount of sample. Diffraction patterns were recorded in the range of scattering angle 2θ 3°–90°, step 0.008°, spectrum collection time 0.1–4.0 s in a point. Several diffraction patterns were obtained under different experimental conditions and different times of spectrum collection.

The obtained data were processed by using the software package EVA[1]. For identifying crystalline phases, the powder metallurgy database (ICDD PDF-2, Release 2005) was used. The complete-profile analysis of diffraction data by the Rietveld method with minimization of the deviation between experimental and theoretical curves was carried in terms of the software packgage TOPAS[2], the convergence parameter *Rwp* was 6.87. Based on the refined data, the size characteristics of silver grains were calculated by several methods.

UV-visible spectra were collected on spectrometer Perkin-Elmer Lambda 25.

RESULTS AND DISCUSSION

AgCl@CTA$^+$ Nanospheres in the Absence of Mediator

The synthesized aqueous solution of AgCl@CTA$^+$ nanospheres was studied by DLS and CV methods, as well as the aqueous solutions of CTACl (0.02 M) and AgCl (0.4 g/L) for comparison.

DLS studies. For CTACl, we observed nanoparticles with the average size of 14 nm (polydispersity index (**PdI**) 0.493) (Fig. 1a); for AgCl, nanoparticles with diameter of 248 nm (PdI 0.190) were observed (Fig. 1b). In the AgCl–CTACl system, no nanoparticles of individual components were observed and those observed were of the different size (331 nm) (PdI 0.376) (Fig. 1c). Naturally, AgCl nanoparticles can bind the surface-active cations CTA$^+$ to afford new coarser particles which, according to [33], represent AgCl@CTA$^+$ nanospheres.

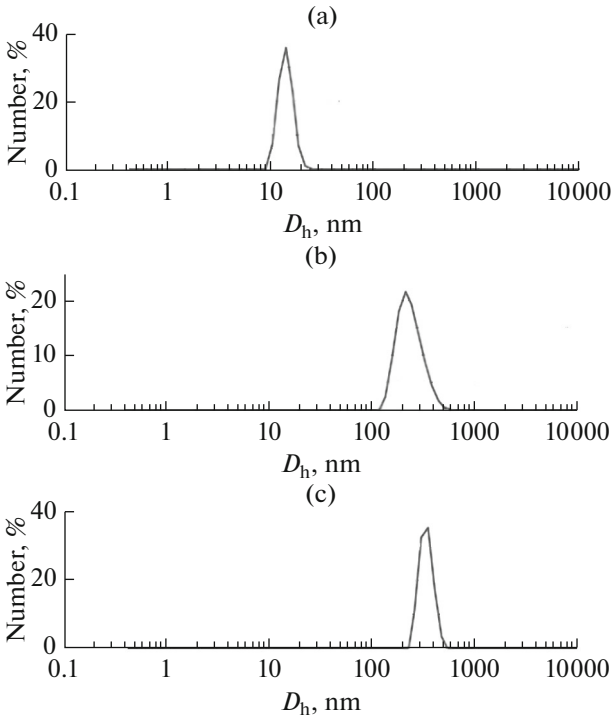

Fig. 1. Diagram of size distribution for (a) CTAC NP (0.02 M). AgCl NP (0.4 g/L), (c) AgCl@CTA$^+$ NP in water.

CV studies. In water, CTACl (0.02 M) is neither oxidized nor reduced in the accessible potential range from −1.40 to +1.00 V. The CV of AgCl (0.4 g/L) (supporting electrolyte: 15.9 mM NaCl + 2.8 mM $NaNO_3$) demonstrate a spread-out peak of AgCl reduction with oscillations (C_1) and, in the reverse scan, a peak corresponding to reoxidation of the metal silver deposit A_1 (E_{A1} = 0.22 V) (Fig. 2a, curve *1*). In multicycle voltammograms, the cathodic branch is transformed: the spread-out peak is replaced by a clear adsorption peak of AgCl reduction (C_1') at −0.09 V (Fig. 2a, curves *3*–*5*). With the increase in the cycle number, the heights of cathodic and anodic peaks gradually decrease.

The electrode exposure at the potential of AgCl reduction (−0.50 V) virtually does not change the peak of adsorbed silver oxidation (A_1) (Fig. 2b). From these results, it follows that only AgCl nanoparticles originally deposited on the electrode during solution stirring are reduced on the electrode. Colloidal AgCl which gradually precipitates and during CV measurements is present in solution as the precipitate is not reduced.

The CV curve of the aqueous solution of AgCl@CTA$^+$ nanospheres prepared by the above procedure demonstrates a much less intense peak of AgCl reduction (C_1), which lacks clear maximum, demonstrating only the current ascending region at E =

[1] EVA v.11.0.0.3. User Manual. SOCABIM 2005.
[2] TOPAS/TOPAS R/TOPAS P. User Manual. BRUKER. AXS GmbH, Karlsruhe, West Germany, 2005.

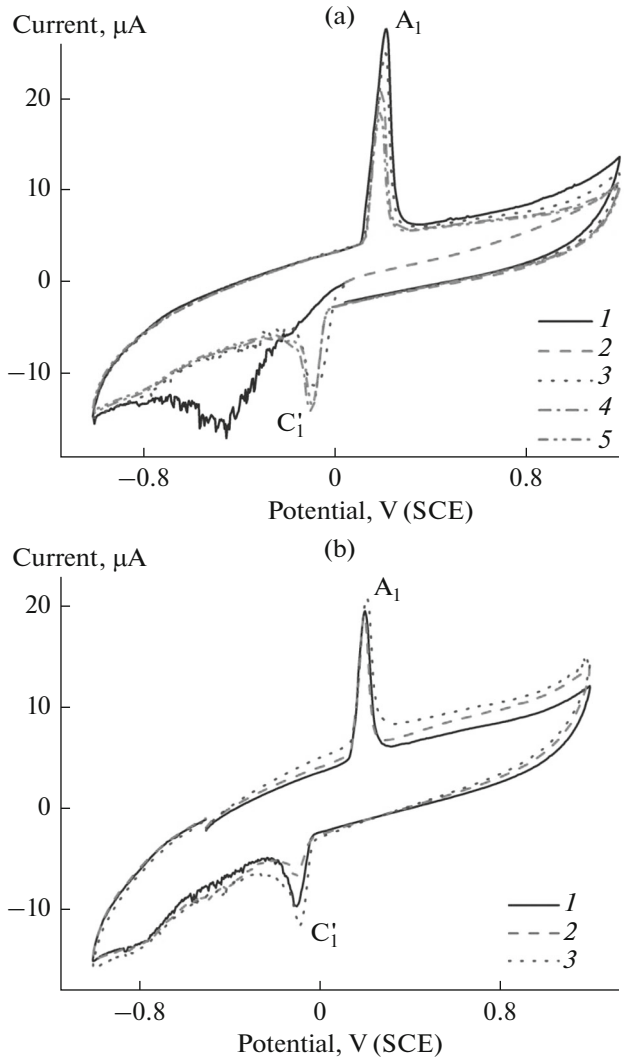

Fig. 2. CV curves of AgCl (0.4 g/L) in the medium of water/0.0158 NaCl–0.0028 M $NaNO_3$: (a) with initial potential scanning in (*1, 3–5*) cathodic and (*2*) anodic direction: (*1*) 1st, (*3*) 2nd, (*4*) 4th, and (*5*) 6th cycles, E_{in} = 0.05 V; (b) after electrode exposure at E = –0.5 V for (*1*) 1, (*2*) 2, and (*3*) 3 min, E_{in} = –0.5 V. v = 100 mV/s.

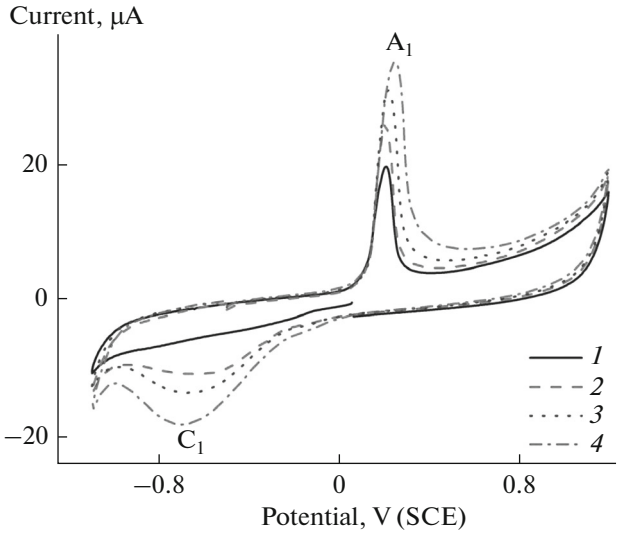

Fig. 3. CV curves of AgCl@CTA^+ nanospheres in the medium of water/0.0187 M CTACl: (*1*) original solution, E_{in} = 0.05 V and after electrode exposure at E = –0.5 V for (*2*) 1, (*3*) 2, and (*4*) 3 min, E_{in} = –0.5 V. v = 100 mV/s.

–(0.11–0.30) V. In the reverse scan, a conjugated reoxidation peak A_1 of metal silver deposited on the electrode is observed at E_p = 0.21 V (Fig. 3, curve *1*). After 1-min electrode exposure at the potential of AgCl reduction (E = –0.5 V), the reoxidation peak height increases; the prolonged exposure leads to the further increase in its height (Fig. 3, curves *2–4*). It is evident that here, in contrast to AgCl, it is the AgCl nanoparticles nondeposited on the electrode but dissolved and delivered to the electrode surface by diffusion that are reduced. This result is an additional argument for the existence of AgCl in solution exclusively as AgCl@CTA^+ and the reduction of the latter particles on the electrode. Nanospheres are sufficiently large (~330 nm) and have correspondingly a low diffusion coefficient; hence, their reduction current is very low. For the same potential scan rates, their current in the peak is ~50 time lower than the reduction current of $AgNO_3$ of the same concentration, i.e., the silver ions bound into AgCl@CTA^+ nanospheres are reduced at a very low rate immediately on the electrode. The resulting metal silver is deposited on the electrode. It should also be mentioned that in the presence of AgCl@CTA^+ the reduction of the supporting electrolyte begins already at the potential of –1.10 V, i.e., the deposition of metal silver on the GC electrode during the CV measurements makes easier the supporting electrolyte reduction by ~0.30 V.

AgCl@CTA^+ Nanospheres in the Presence of Methylviologen as the Mediator

CV studies of methylviolgen. The CV curve of methylviologen (2 mM) in the water/0.02 M CTACl medium demonstrates three reduction peaks C_2, C_2' and C_3 (E_{C2} = –0.79 V, $E_{C2'}$ = –0.98 V, E_{C3} = –1.11 V) and two reverse peaks of reoxidation A_2 and A_3 (E_{A2} = –0.56 V, E_{A3} = –0.86 V) (Fig. 4a). If in place of CTACl we use NaCl of the same concentration, we observe two reversible one-electron peaks typical of MV^{2+} reduction to $MV^{\bullet+}$ radical cation and neutral diamine MV^0 C_2 and C_3, respectively (E_{C2} = –0.87 V, E_{C3} = –1.29 V, E_{A2} = –0.51 V, E_{A3}= –0.73 V) (Fig. 4b). The ($E_p - E_{p/2}$) value and the potential difference between the reduction and reoxidation peaks exceed the theoretical value for a one-electron reversible processes, which is explained by the large voltage drop iR due to the low concentration of the supporting electrolyte. As regards their potentials, the reduction peaks on this background correspond to peaks C_2 and C_3, and the

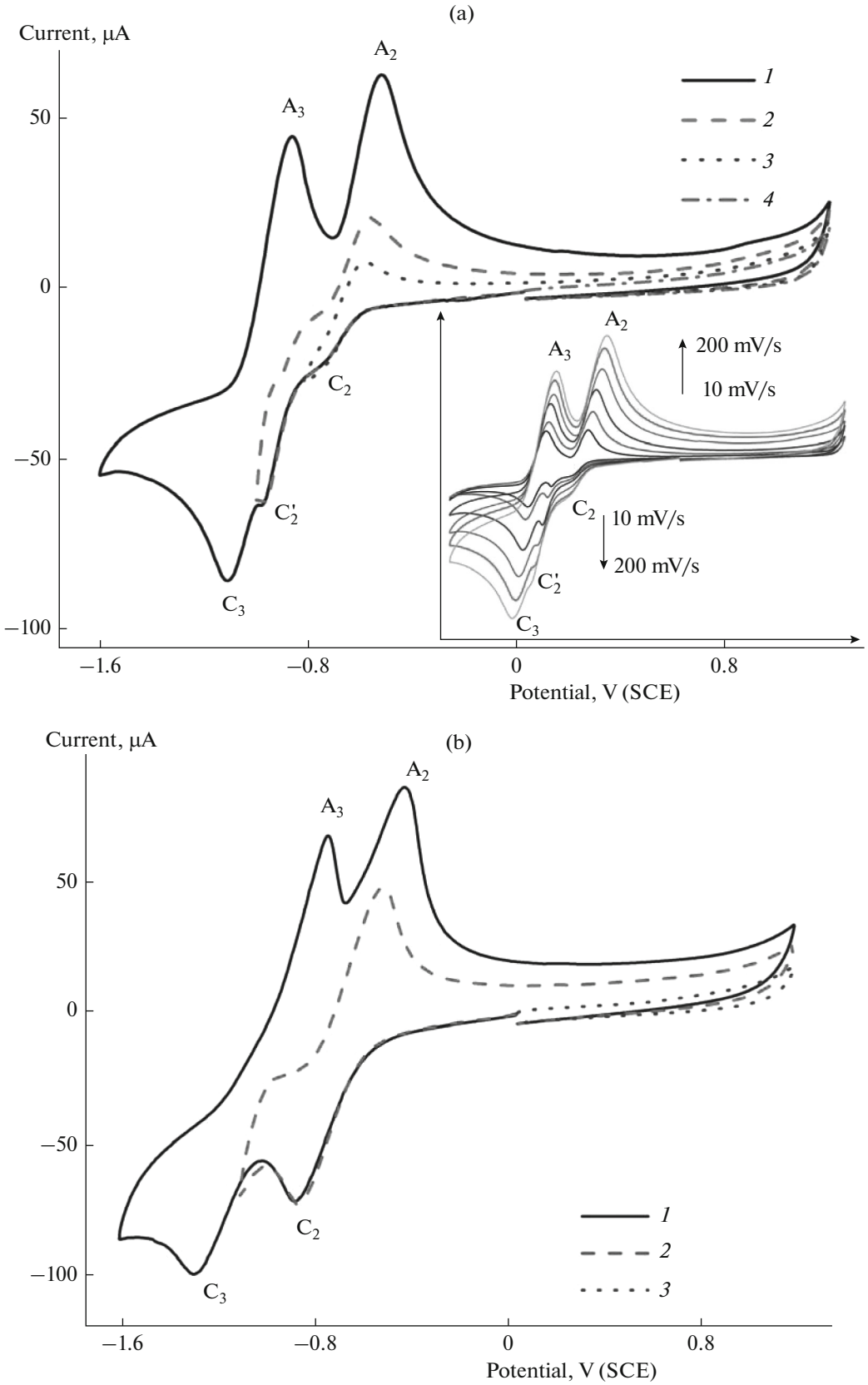

Fig. 4. CV curve of MV^{2+} (2 mM) (a) in the medium of water/0.02 M CTACl with initial potential scanning into (*1–4*) cathodic and (*5*) anodic direction. Insert: at different potential scan rates *v*, mV/s: (*1*) 10, (*2*) 20, (*3*) 50, (*4*) 100, (*5*) 150, (*6*) 200, $E_{in} = 0.03$ V; (b) in water/0.02 M NaCl medium with initial potential scanning in (*1–2*) cathodic and (*3*) anodic direction, $E_{in} = 0.05$ V. $v = 100$ mV/s.

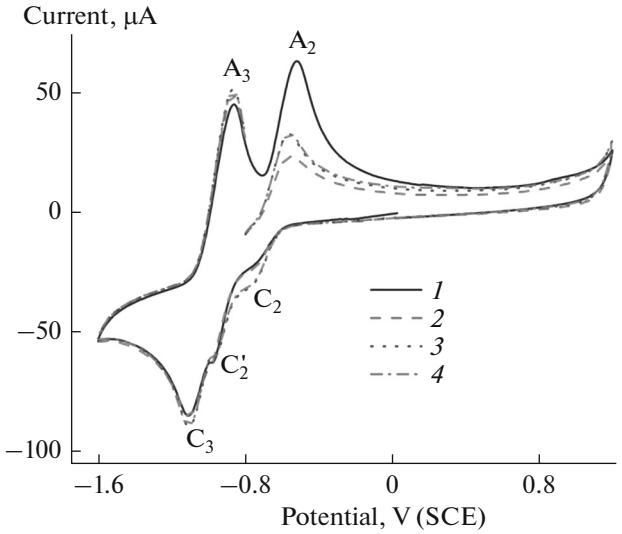

Fig. 5. CV curves of MV^{2+} (2 mM) in the medium of water/0.02 M CTACl: (*1*) original solution (E_{in} = 0.03 V) and after electrode exposure at E = –0.80 V for (*2*) 1, (*3*) 2, and (*4*) 3 min (E_{in} = –0.80 V). v = 100 mV/s.

reoxidation peaks correspond to reoxidation peaks by the background of CTACl. (The complete coincidence of potentials is impossible because CTACl exists in solution as micelles so that the solution conductivity differs from that of a NaCl solution of the same concentration). Hence, MV^{2+} is partly bound in the CTACl micelles and the bound form of MV^{2+} is reduced at potentials of peak C_2'. The resulting radical cations quickly and quantitatively leave the micelles so that their further reduction and reoxidation proceed from the unbound state.

The presence of individual peaks for MV^{2+} bound in micelles (C_2') and unbound (C_2) points to the low mobility of equilibrium between them. According to Fig. 4a (insert), as the potential scan rate decreases, the ratio of heights of peaks C_2 and C_2' increases. Thus, peak C_2' is much lower than C_2 at potential scan rates of 10, 20 mV/s and their heights become virtually equal at 100 mV/s. Insofar as the potential scan rate is inversely proportional to the time for reduction and the ratio of peak heights is related to the ratio of concentrations of the reduced substance from its unbound and bound states, this can be formulated differently: as the time for reduction of the methylviologen unbound form increases, the fraction of substance reduced from this form also increases. This means that this not too mobile equilibrium is sufficiently mobile for shifting considerably according to the Le Chatelier principle if one considers the CV curves on the time scale.

The electrode exposure at the potential of reduction peak C_2 (E = –0.80 V) does not induce any considerable change in the height of the radical cation reduction peak (Fig. 5); this means that in this medium, the $MV^{\bullet+}$ radical cation is not adsorbed on the electrode surface. Hence, the stage of AgCl reduction by $MV^{\bullet+}$ radical cation proceeds not on the electrode surface but in solution bulk, which favors the synthesis of metal nanoparticles in solution bulk.

CV Studies of the AgCl@CTA$^+$ Nanosphere in the Presence of Methylviologen

The morphology of the CV curve of this system substantially differs from that of the summarized curve of methylviologen and AgCl@CTA$^+$ nanospheres taken separately (Fig. 6a). The difference is that the methylviologen curve lacks the reduction peak C_2' and the intensities of the other two peaks are approximately twice higher, whereas the heights of the reverse peaks of its reoxidation are virtually the same. Moreover, in the anodic region an additional reoxidation peak A_4 appears at E_p = 0.84 V if the reversal occurs after the second reduction peak (Fig. 6a).

Electrode exposure at the potential of AgCl reduction (E = –0.50 V) increases the peak of oxidation of generated Ag^0 (A_1) (Fig. 6b), while for its exposure at the potential of the methylviologen reduction peak C_2 (E = –0.80 V), the oxidation currents of generated $MV^{\bullet+}$ and Ag^0 are independent of the exposure time (Fig. 6c). In this case, the peak A_1 of Ag^0 oxidation (E_p = 0.14 V) is very weak. It deserves mention that at the exposure at both potentials (E = –0.5 and –0.8 V), three peaks of MV^{2+} reduction are observed in the reverse cathodic branch, i.e., the CV curve of methylviologen has the same form as in the absence of AgCl.

In aggregate, the obtained data can be interpreted as follows. In the aqueous CTACl solution both in the presence and in the absence of methylviologen, silver chloride takes the form of AgCl@CTA$^+$ nanospheres that are not adsorbed on the electrode and are reduced at a very low rate due to their low mobility. The reduction product is metal silver deposited on the electrode and oxidized at E_p = 0.16 V. As to the state of methylviologen, it changes radically in the presence of AgCl where methylviologen is in the free state. This suggests that CTA^+ cations are completely bound in AgCl@CTA$^+$ nanospheres and that nanospheres fail to bind methylviologen. Thus, in the CV curve the peak of methylviologen bound form is absent (peak C_2' in the absence of AgCl) and, correspondingly, the height of peak C_2 doubles. As to the increase in the peak C_3 height, we attribute this to superposition of the current from the supporting electrolyte reduction which in the presence of AgCl@CTA$^+$ nanospheres starts at –1.10 V. The supporting electrolyte reduction results in the appearance in solution of free and/or micelle-bound hydroxide ions. The oxidation of the latter explains the appearance of the reoxidation peak A_4 at E_{A4} = 0.84 V.

Methylviologen radical cations generated by the reduction of free methylviologen are neither bound in

micelles nor adsorbed on the electrode but reduce AgCl in AgCl@CTA$^+$ nanospheres in solution volume (Scheme). This determines the growth of two first peaks of methylviologen reduction C_2 and C_2', the decrease in the reoxidation peak of its radical cations A_2, and the small amount of metal deposited on the electrode when the latter is kept at potential of radical cation generation (–0.80 V). The metal deposition takes place only in the initial moment of electrolysis when nanospheres are reduced immediately on the electrode. Later, they are reduced by the mediator mechanism in solution volume and cease to be deposited on the electrode. After the reduction of AgCl@CTA$^+$ nanospheres, the oxidation of deposited Ag^0, and the subsequent reduction of AgCl formed, the liberated CTA$^+$ cations bind methylviologen; this is why the CV of methylviologen shows the peak of reduction of its bound form C_2' (Figs. 6b, 6c).

Thus, these results are the voltammetric evidence that the mediated electroreduction of AgCl@CTA$^+$ nanospheres can produce metal nanoparticles in solution volume at potentials of generation of methylviologen radical cations.

Preparative Mediated Electrosynthesis of Ag@CTA$^+$ Nanoparticles

For preparative electroreduction, we used a solution of the same composition as for voltammetric studies; the CV curve measured in this solution is identical that shown above (Fig. 6a). The electrolysis was carried out at the potential of the peak of methylviologen reduction E_{C2} = –0.92 V. During the electrolysis, blue stains of $MV^{\bullet+}$ radical cations evolved from the glassy carbon plate used as the cathode and quickly disappeared in solution bulk. The original opaque white solutions immediately started to transform into yellow, which is typical of metal silver nanoparticles. In time, the yellow color intensified and the solution became yellowish brown. After the theoretical charge was passed, a green tint appeared and at 18% excess of charge the solution acquired the blue color typical of methylviologen radical cations. This pointed to the complete reduction of AgCl in the system and the appearance of a large amount of $MV^{\bullet+}$ in solution. This is why the electrolysis was stopped. Excessive $MV^{\bullet+}$ was reoxidized by air oxygen. As a result, we obtained a homogeneous yellowish-brown solution. In is evident that the quantitative reduction of AgCl occurs once the theoretical charge has been passed and green color has appeared due to superposition of blue from methyviologen radical cations on yellowish-brown. It is interesting that during the period of electrolysis (31 min), the current did not decrease as it usually does at electrolysis but on the contrary increased from –3.3 to –4.6 mA.

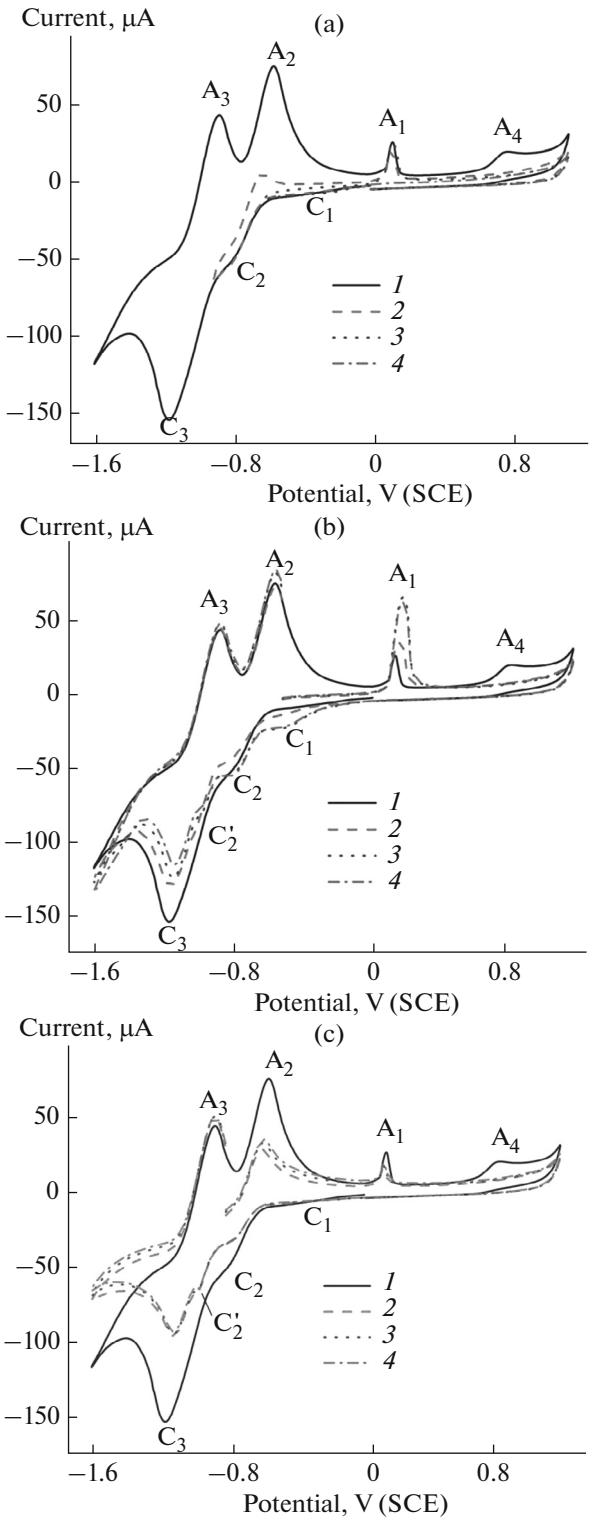

Fig. 6. CV curves of the MV^{2+} (1.87 mM)–AgCl (0.4 g/L) system in the medium of water/0.0187 M CTACl: (a) with initial potential scanning in (*1*–*4*) cathodic and (*5*) anodic direction, E_{in} = 0.03 V; (b): (1) in initial solution, E_{in} = 0.03 V; (2) after the electrode exposure at E = –0.50 V for 1, (*3*) 2, and (*4*) 3 min, E_{in} = –0.50 V; (c) (*1*) original solution, E_{in} = 0.03 V; (*2*) after electrode exposure at E = –0.80 V for 1, (*3*) 2, (*4*) 3 min, E_{in} = –0.80 V. v = 100 mV/s.

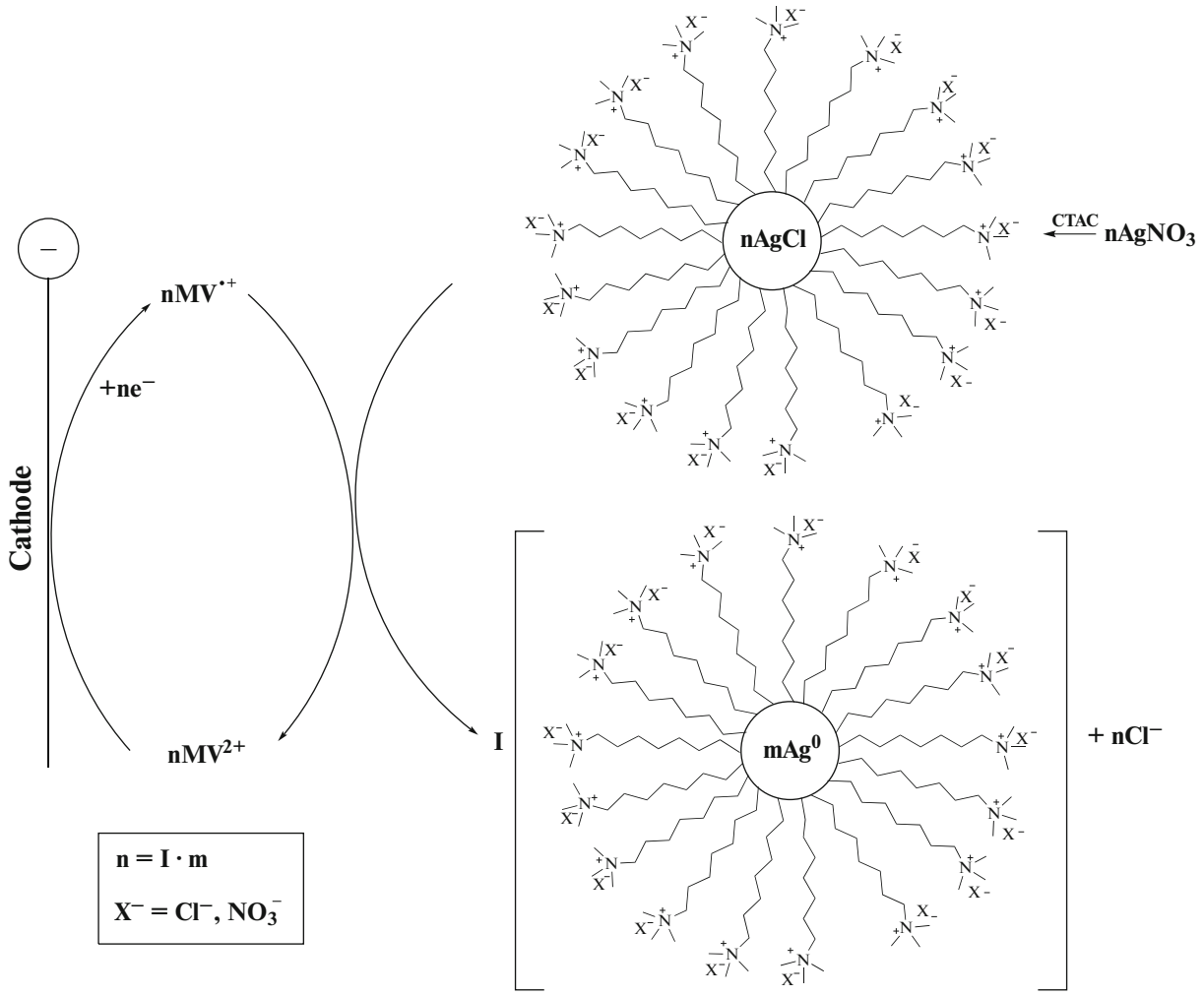

Scheme. Methylviologen-mediated reduction of AgCl@CTA$^+$ nanospheres to form Ag@CTA$^+$ nanoparticles.

The electron spectra of solution after the electrolysis demonstrated a wide twin absorption band with the maximum at 423 nm, usually attributed to silver nanoparticles [34] (Fig. 7). The band in the UV region (256 nm) corresponded to MV^{2+}.

The CV curve in the cathodic region (Fig. 8) is virtually identical to that of methylviologen in the absence of AgCl in solution (Fig. 4a). The synthesized silver nanoparticles were neither adsorbed nor deposited on the glassy carbon electrode. This was indicated by the constant weight of the cathode during electrolysis and the absence of Ag^0 oxidation peak when the electrode was exposed for 3 min to solution at open circuit without stirring. After the electrolysis, in the anodic region, a peak appeared at $E_{A4} = 0.86$ V (Fig. 8) which corresponded to oxidation of hydroxide ions formed in the reaction of oxygen with the excessive amount of generated methylviologen radical cations.

The DLS data indicated that the electrolysis solution contained polydisperse (PdI = 0.506) nanoparticles: as regards intensity, the average size of particles was 8 nm (11%) and 77 nm (89%), and as regards the number, the average size was 5.3 nm (100%) (Fig. 9). Only coarser particles (77 nm) can be unambiguously attributed to metal nanoparticles stabilized by CTACl, whereas the finer particles may represent both metal particles and CTACl micelles.

The results of analysis of the deposit isolated from solution by the method of powder X-ray diffraction unambiguously pointed to the presence of crystalline silver Ag^0. According to the obtained data, the suspension sample represented a mixture of crystalline substances, which included the cubic form of crystalline silver[3] the interference peaks of which substantially differ as regards their shape and width from the other peaks present in the diffraction pattern (Fig. 10).

Assuming that the additional crystalline components in the sample could be either methylviologen dichloride or cetyltrimethylammonium chloride, we

[3] Silver, syn., code № 01-087-0720 (I), according to the Database of powder diffractometry PDF-4.

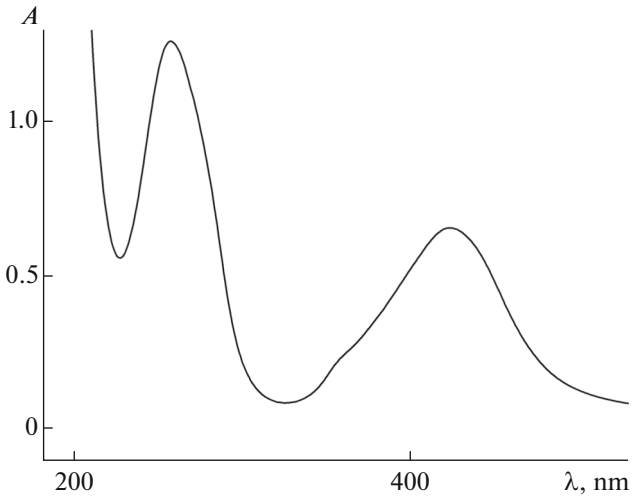

Fig. 7. UV-visible spectrum of MV^{2+} (1.87 mM)–AgCl (0.4 g/L) in the medium of water/0.0187 M CTACl after the reduction at $E = -0.92$ V followed by 40-fold solution dilution with water.

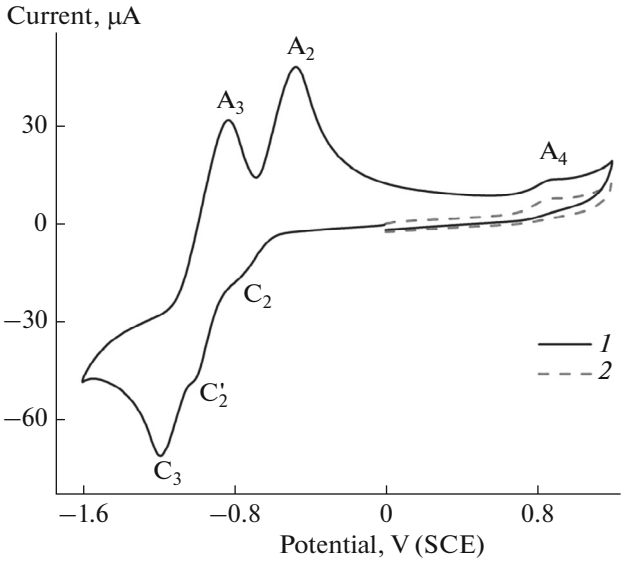

Fig. 8. CV curves of the MV^{2+} (1.87 mM)–AgCl (0.4 g/L) system in the medium of water/0.0187 M CTACl after electrolysis at $E = -0.92$ V ($Q = 1.18$ F rated for AgCl) with the initial potential scanning in (*1*) cathodic and (*2*) anodic direction. $E_{in} = 0.00$ V. $v = 100$ mV/s.

carried out the corresponding XRPD experiments with these compounds; the experimental curves are shown in Fig. 10. These figure also shows the positions of diffraction peaks of silver chloride; however, the comparison of diffraction patterns points to the absence of these substances in the suspension.

The size of coherent scattering regions, i.e., the smallest crystalline domains constituting silver particles or crystals, was calculated with the use of the software package TOPAS2 by several methods: the values calculated from the half-width of reflexes (LVol-FWHM) and from the integral intensity of reflexes (LVol-IB) represent the grain size weight-averaged throughout the volume and parameter CrySizeG is the grain size in the direction normal to analyzed planes for the Gaussian type of broadening (table).

The obtained data (table) indicate that the sample is nanostructural because its average grain size is 8–16 nm. The analysis of the data makes it possible to note that the grain size in the direction normal to this family of planes turns out to be sufficiently close to their size found by different methods of calculation. To a certain degree, the average grain size characterizes the shape of grains or the degree of its deviation from the sphere, because, for example, for spherical grains this value should coincide with the size calculated only in a certain direction. In our case, the grain shape can be assumed to be close to globular.

According to the SEM data, the main size of isolated nanoparticles is 39 ±15 nm (Fig. 11a). The STEM image shows that not only metal nanospheres with the average size of 34 ± 24 nm and nonideal shape are formed but also a small number of nanorods of various diameters (13–22 nm) and various lengths (reach 85 nm and more) (Fig. 11b). The ratio of nanorods to nanospheres is about 1 : 25.

The energy-dispersion spectrum of particles (Fig. 12) shows the presence of silver, chlorine, and carbon. It is obvious that a sufficiently large number of CTACl is bound with silver nanoparticles and they are deposited together at their evolution. The positive charge of particles dispersed in water agrees with this conclusion, as follows from the average zeta potential +74.6 mV.

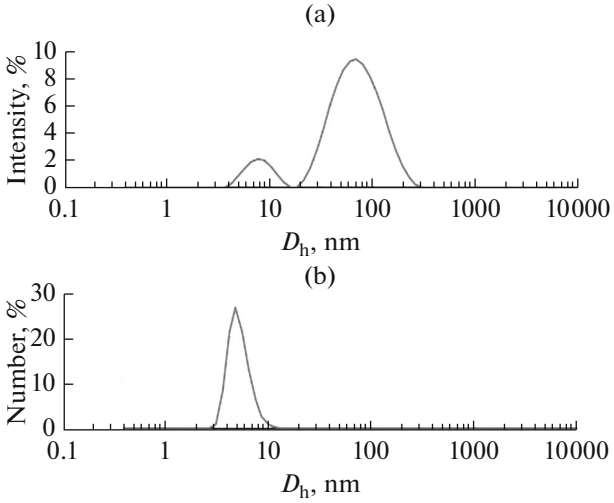

Fig. 9. Diagrams of size distribution for silver NP stabilized by CTAC in water: (a) with respect to intensity, (b) with respect to number.

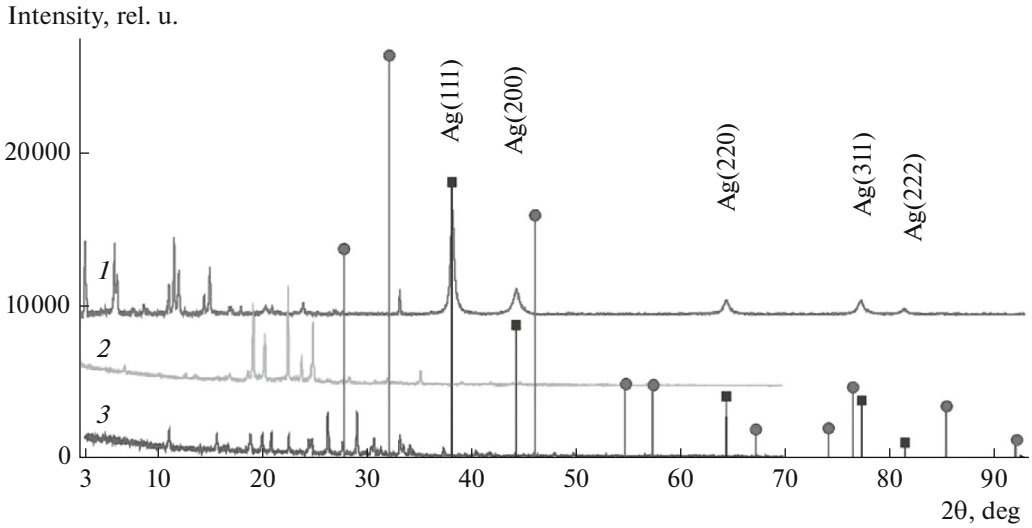

Fig. 10. Experimental diffraction patterns of (*1*) suspension sample after correction for the background scattering, (*2*) CTACl, and (*3*) methylviologen. The position of interference peaks corresponding to crystalline silver (Silver, syn., code no. 01-087-0720) is indicated by vertical lines marked with squares with plane indices. For a comparison, the vertical lines marked with circles show the positions of interference peaks corresponding to the crystalline form of silver chloride (code no. 01-085-1355). For better visualization, the curves are shifted with respect to one another along the intensity axis.

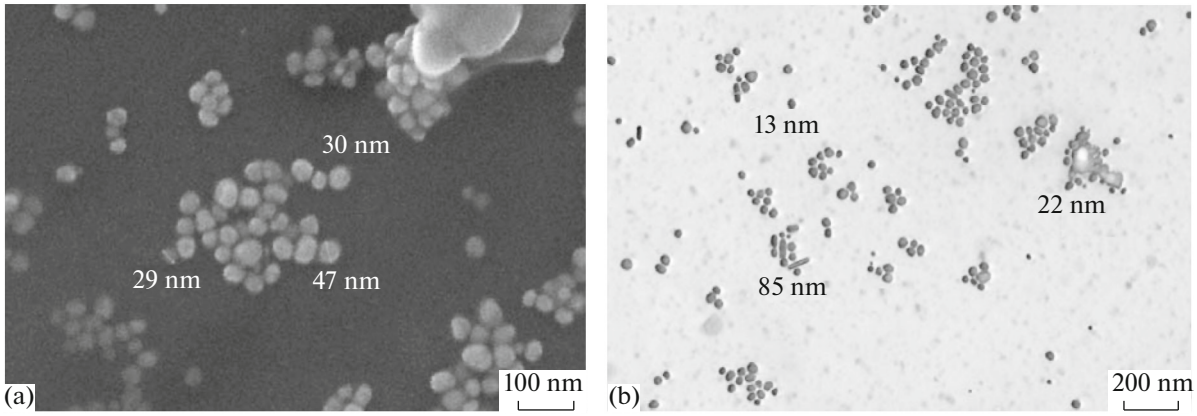

Fig. 11. (a) SEM and (b) STEM images of silver nanoparticles stabilized by CTACl.

Thus, the methylviologen-mediated electroreduction of AgCl@CTA$^+$ nanospheres in aqueous medium produces silver nanospheres stabilized by CTA$^+$ cations adsorbed on their surface (AgCl@CTA$^+$). Their reduction leads to a decrease in the nanoparticle size from 330 nm for AgCl@CTACl to 39 nm for Ag@CTACl. Such a strong change in the particle size is apparently associated not only with the escape of chloride ions from the nanoparticle composition and modifications in their structure

Size of silver grains calculated from peak parameters

Miller indices of peak	111	200	220	311	222
Angle 2θ, deg	38.287(1)	44.434(4)	64.611(5)	77.528(5)	81.65(1)
I, rel. u.	232(1)	139(1)	149(1)	206(3)	67(1)
CrySizeG, nm	16.02(8)	8.74(8)	11.4(2)	12.2(2)	15.5(5)
LVol-IB, nm	15.05(7)	8.21(8)	10.7(2)	11.4(2)	14.6(5)
Lvol-FWHM, nm	14.26(7)	7.78(7)	10.1(1)	10.8(2)	13.8(5)

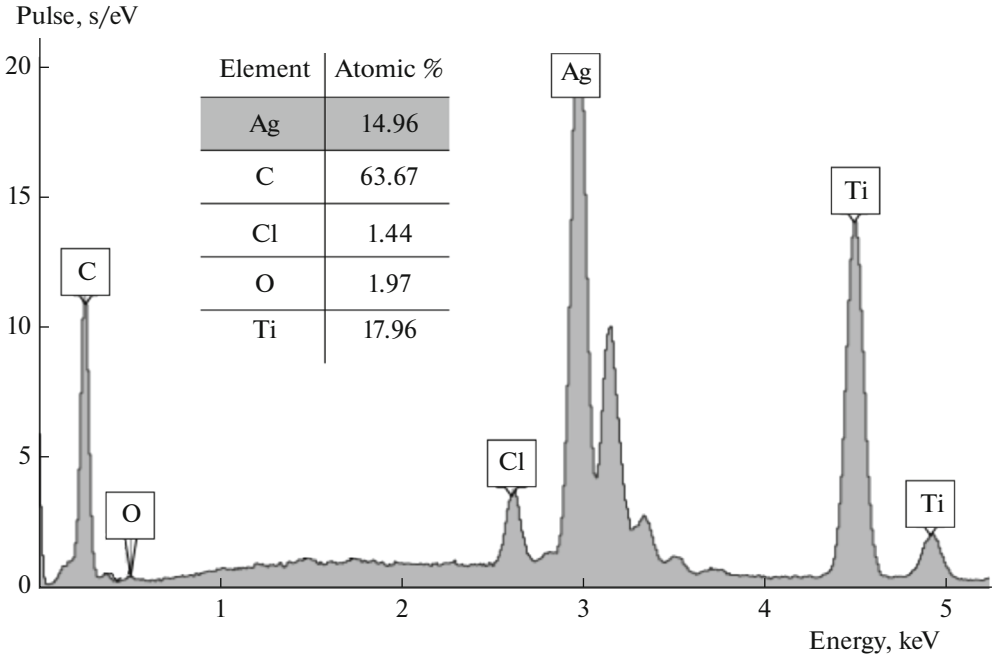

Fig. 12. Energy-dispersion spectrum of silver nanoparticles stabilized by CTACl on a titanum support.

from loose to denser but also with another restructuring leading to formation of several Ag@CTA$^+$ nanoparticles from one AgCl@CTA$^+$ nanosphere (Scheme).

For a comparison and also as an additional substantiation to the role of CTA$^+$ cations in stabilization of metal nanoparticles, we carried out analogous electrosynthesis of metal nanoparticles in the absence of CTACl by changing the latter by NaCl of the same concentration.

Mediated Electrosynthesis of Ag Nanoparticles in the Absence of CTACl.

After a certain period upon the addition of methylviologen (1.87 mM) to the colloid solution of AgCl (for synthesis and composition, see Experimental), the solution became transparent and a white coarse-grained sediment appeared on the bottom. Colloid solution was obtained again by supersonic treatment but in several seconds after its cessation virtually all AgCl precipitated. It should be noted that in the presence of CTA$^+$ we failed to observe such an effect of MV^{2+} on the precipitation of AgCl dispersion, which can be considered as an additional argument for stabilization of AgCl nanoparticles by CTA$^+$ cations.

The CV curves of this system demonstrate four reduction peaks ($E_{C1'} = -0.15$, $E_{C1} = -0.63$, $E_{C2} = -0.93$, and $E_{C3} = -1.32$ V) (Fig. 13a), where the latter two peaks pertain to reversible two-step reduction of methylviologen. Due to precipitation, the heights of the first two peaks are poorly reproducible and they are often virtually indiscernible but sometimes can be seen (Fig. 13a). In the reverse potential scan started from the first weakly pronounced peak C_1', the peak of reoxidation of Ag^0 deposited on the electrode (A_1) appears (Fig. 13a). As the reduction time is increased by electrode exposure at $E = -0.3$ V, this peak grows and a peak of reduction of adsorbed AgCl (C_1') appears in the reverse branch at -0.10 V (Fig. 13b). It is evident that in the presence of methylviologen, AgCl is not deposited quantitatively and remains partly in solution to be reduced at potentials of the first peak.

If the scan reversal occurs at the second reduction peak C_1, the reverse branch contains only the peak of reoxidation of deposited silver A_1 (Fig. 13c). As the time of reduction at -0.60 V increases, the amount of deposited metal also increases; moreover, this amount is larger as compared with the reduction at potentials of peak C_1'. This means that at the C_1 peak potential, AgCl is also in its reduced form. However, it is unclear how it was reduced: immediately on the electrode or by the mediated process with electrochemically generated methylviologen radical cations as in case of $[PdCl_4]^{2-}$ [23–25].

As in the previous system with CTA$^+$, methylviologen MV^{2+} serves as the mediator at the potentials of radical cation generation. This follows from the fact that the peak of oxidation of deposited metal silver decreases when the electrode is exposed at potential of the first reduction peak of methylviologen C_2 (-0.80 V) (Fig. 13d). However, in this system, in contrast to the previous one, the radical cations $MV^{\bullet+}$ are adsorbed

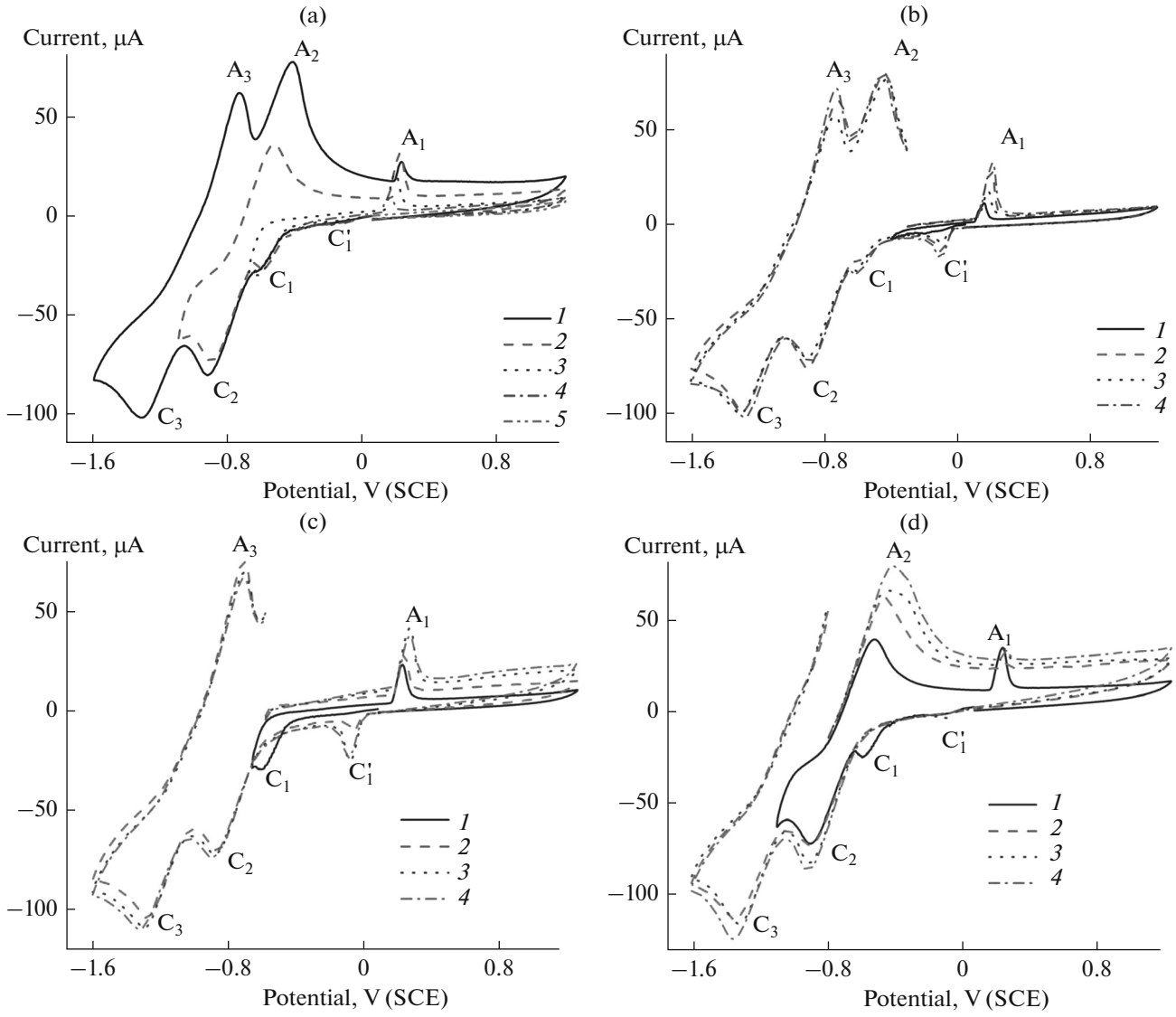

Fig. 13. CV curves of the system MV^{2+} (1.87 mM)–AgCl (0.4 g/L) in the medium of water/0.0158 M NaCl–0.0028 M $NaNO_3$ (a) with initial potential scanning in (*1*–*4*) cathodic and (*5*) anodic direction, E_{in} = 0.05 V; (b) (*1*) original solution, E_{in} = 0.05 V; after electrode exposure at E = –0.30 V (*2*) for 1, (*3*) 2, and (*4*) 3 min, E_{in} = –0.30 V; (c) (*1*) original solution, E_{in} = 0.05 V and after electrode exposure at E = –0.60 V for (*2*) 1, (*3*) 2, and (*4*) 3 min, E_{in} = –0.60 V; (d) (*1*) original solution, E_{in} = 0.05 V; after electrode exposure at E = –0.80 V for (*2*) 1, (*3*) 2, and (*4*) 3 min, E_{in} = –0.80 V. v = 100 mV/s.

on the electrode, inducing the growth of their oxidation peak A_2 with the increase in reduction time (Fig. 13d).

Preparative methylviologen-mediated electroreduction of AgCl was carried out at the controlled potential E = –1.0 V. From the very beginning of electrolysis, the solution started to become blue, i.e., took the color of radical cations $MV^{\bullet+}$, and gradually all solution acquired blue color and its intensity increased. During the electrolysis, the current gradually decreased, the theoretical charge was passed in 13 min, and the final solution was dark blue. After the end of electrolysis, solution was stirred for 15 min; in the process, its color disappeared and coarse agglomerates of dark metal particles were formed on the bottom; no white AgCl deposit was left in the system. The generated metal was not deposited but remained completely in solution, which followed from the invariant electrode mass during the electrolysis.

At supersonic treatment, the formed agglomerates were broken and the solution became opaque. The precipitate was separated from solution by centrifugation, washed with water, and dispersed in water by sonication. The resulting suspension quickly precipitated as coarse particles. Nonetheless, the DLS method revealed the presence of micrometer particles

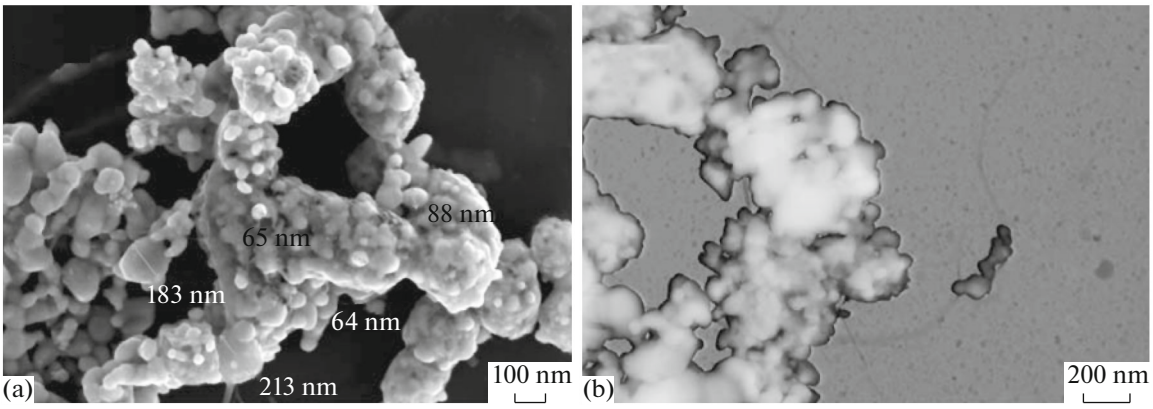

Fig. 14. (a) SEM and (b) STEM images of metal silver synthesized without stabilizer.

in solution (1096 nm as regards intensity and 1091 nm as regards number, PdI = 0.545).

SEM and STEM studies demonstrated that metal silver in suspension was not nanosized but represented coarse agglomerates of adhered particles of different size and shape (Fig. 14). The energy-dispersion spectrum showed that the particles mainly contained only silver (56.89 at %).

CONCLUSIONS

In this study, we demonstrated experimentally the possibility of efficient mediated electrosynthesis of metal nanoparticles from their salts encapsulated in micelles by the example of silver NP in aqueous medium by methylviologen-mediated reduction of AgCl nanospheres stabilized in shells of surface-active cetyltrimethylammonium cations ($AgCl@CTA^+$). Nanospheres $AgCl@CTA^+$ (~330 nm) can be reduced on the glassy carbon electrode at a very low rate and generated metal is deposited on the electrode. For the mediated reduction at the potential of the $MV^{2+}/MV^{\bullet+}$ redox couple, the process is fast, the metal is not deposited on the cathode, and at $Q = 1$ F the quantitative reduction of AgCl to Ag@CTACl particles (39 ± 15 nm) proceeds in the solution bulk. The average size of metal grains in these particles is 8–16 nm. In solution, the metal nanoparticles exist in the form of $Ag@CTA^+$, as follows from the value of their electrokinetic (zeta) potential (74.6 mV). The positive charge keeps them from agglomeration. Nanoparticles were characterized by the methods of UV spectroscopy, XRPD, and electron microscopy (SEM, STEM). It is noteworthy that the metal forms not only nanospheres but also a small number of nanorods. In the absence of CTACl, the analogous methylviologen-mediated reduction of AgCl also proceeds efficiently but produces only micrometer metal particles that form aggregates and are of various shapes.

ACKNOWLEDGMENTS

This study was financially supported by the Russian Foundation for Basic Research (projects nos. 14-03-00405a and 16-33-00420 mol_a.

REFERENCES

1. Pomogailo, A.D., Rozenberg, A.S., and Uflyand, I.E., *Nanochastitsy metallov v polimerakh (Metal Nanoparticles in Polymers)*, Moscow: Khimiya, 2000.
2. Roldugin, V.I., *Russ. Chem. Rev.,* 2000, vol. 69, p. 821.
3. Daniel, M.C. and Astruc, D., *Chem. Rev.,* 2004, vol. 104, p. 293.
4. Suzdalev, I.P., *Nanotekhnologiya: Fiziko-khimiya nanoklasterov, nanostruktur i nanomaterialov (Nanotechnology: Physical Chemistry of Nanoclusters, Nanostructures, and Nanomaterials)*, 2nd Ed., Librokom, 2009.
5. Volkov, V.V., Kravchenko, T.A., and Roldugin, V.I., *Russ. Chem. Rev.,* 2013, vol. 82, p. 465.
6. Dykman, L.A., Bogatyrev, V.A., Shchegolev, S.Yu., and Khlebtsov, N.G., *Zolotye nanochastitsy. Sintez, svoistva, biomeditsinskoe primenenie (Gold Nanoparticles. Synthesis, Properties, and Applications in Biomedicine)*, Moscow: Nauka, 2008.
7. Kharisov, B.I., Kharissova, O.V., and Ortiz-Méndez, U., *Handbook of Less-Common Nanostructures,* CRC Press, Taylor Francis Group, 2012.
8. Rodrigues-Sanchez, L., Blanko, M.L., and Lopez-Quintela, M.A., *J. Phys. Chem.,* 2000, vol. 104, p. 9683.
9. Yin, B., Ma, H., Wang, S., and Chen, S., *J. Phys. Chem. B,* 2003, vol. 107, p. 8898.
10. Saez, V. and Mason, T.J., *Molecules,* 2009, vol. 14, p. 4284.
11. Zhu, J., Liu, S., Palchik, O., Koltypin, Y., and Gedanken, A., *Langmuir,* 2000, vol. 16, p. 6396.
12. Reisse, J., Caulier, T., Deckerkheer, C., Fabre, O., Vandercammen, J., Delplancke, J.L., and Winand, R., *Ultrason. Sonochem.,* 1996, vol. 3, p. S147.
13. Reetz, M.T. and Helbig, W., *J. Am. Chem. Soc.,* 1994, vol. 116, p. 7401.

14. Becker, J.A., Schäfer, R., Festag, R., Ruland, W., Wendorff, J.H., Pebler, J., Quaiser, S.A., Helbig, W., and Reetz, M.T., *J. Chem. Phys.,* 1995, vol. 103, p. 2520.
15. Reetz, M.T., Quaiser, S.A., and Merk, C., *Chem. Ber.,* 1996, vol. 129, p. 741.
16. Reetz, M.T., Helbig, W., Quaiser, S.A., Stimming, U., Breuer, N., and Vogel, R., *Science,* 1995, vol. 267, p. 367.
17. Reetz, M.T., Winter, M., Breinbauer, R., Thurn-Albrecht, T., and Vogel, W., *Chem. - Eur. J.,* 2001, vol. 7, p. 1084.
18. Reetz, M.T., Helbig, W., and Quaiser, S.A., *Chem. Mater.,* 1995, vol. 7, p. 2227.
19. Li, Y., Qiang, Q., Zheng, X., and Wang, Z., *Electrochem. Commun.,* 2015, vol. 58, p. 41.
20. Vilar-Vidal, N., Blanco, M.C., López-Quintela, M.A., Rivas, J., and Serra, C., *J. Phys. Chem. C*, 2010, vol. 114, p. 15924.
21. Yu, Y.-Y., Chang, S.-S., Lee, C.-L., and Wang, C.R.C., *J. Phys. Chem. B*, 1997, vol. 101, p. 6661.
22. Mohamed, M.B., Wang, Z.L., and El-Sayed, M.A., *J. Phys. Chem. A,* 1999, vol. 103, p. 10255.
23. Yanilkin, V.V., Nasybullina, G.R., Ziganshina, A.Yu., Nizamiev, I.R., Kadirov, M.K., Korshin, D.E., and Konovalov, A.I., *Mendeleev Commun.,* 2014, vol. 24, p. 108.
24. Yanilkin, V.V., Nasybullina, G.R., Sultanova, E.D., Ziganshina, A.Yu., and Konovalov, A.I., *Russ. Chem. Bull.,* 2014, vol. 63, p. 1409.
25. Yanilkin, V.V., Nastapova, N.V., Nasretdinova, G.R., Mukhitova, R.K., Ziganshina, A.Yu., Nizameev, I.R., and Kadirov, M.K., *Russ. J. Electrochem.,* 2015, vol. 51, p. 951.
26. Fedorenko, S., Jilkin, M., Nastapova, N., Yanilkin, V., Bochkova, O., Buriliov, V., Nizameev, I., Nasretdinova, G., Kadirov, M., Mustafina, A., and Budnikova, Y., *Colloids Surf. A,* 2015, vol. 486, p. 185.
27. Yanilkin, V.V., Nastapova, N.V., Sultanova, E.D., Nasretdinova, G.R., Mukhitova, R.K., Ziganshina, A.Yu., Nizameev, I.R., and Kadirov, M.K., *Russ. Chem. Bull.,* 2016, vol. 65, p. 125.
28. Nasretdinova, G.R., Fazleeva, R.R., Mukhitova, R.K., Nizameev, I.R., Kadirov, M.K., Ziganshina, A.Yu., and Yanilkin, V.V., *Electrochem. Commun.,* 2015, vol. 50, p. 69.
29. Nasretdinova, G.R., Fazleeva, R.R., Mukhitova, R.K., Nizameev, I.R., Kadirov, M.K., Ziganshina, A.Yu., and Yanilkin, V.V., *Russ. J. Electrochem.,* 2015, vol. 51, p. 1029.
30. Yanilkin, V.V., Nastapova, N.V., Nasretdinova, G.R., Fazleeva, R.R., and Osin, Y.N., *Electrochem. Commun.,* 2015, vol. 59, p. 60.
31. Yanilkin, V.V., Nasretdinova, G.R., Osin, Y.N., and Salnikov, V.V., *Electrochim. Acta,* 2015, vol. 168, p. 82.
32. Yanilkin, V.V., Nastapova, N.V., Nasretdinova, G.R., Fedorenko, S.V., Jilkin, M., Mustafina, A.R., Gubaidullin, A.T., and Osin, Y.N., *RSC Adv.,* 2016, vol. 6, p. 1851.
33. Shen, Y., Chen, P., Xiao, D., Chen, Ch., Zhu, M., Li, T., Ma, W., and Liu, M., *Langmuir,* 2015, vol. 31, p. 602.
34. Krutyakov, Yu.A., Kudrinskii, A.A., Olenin, A.Yu., and Lisichkin, G.V., *Russ. Chem. Rev.,* 2008, vol. 77, p. 233.

Translated by T. Ya. Safonova